tron microscopic level (*10*). In contrast to DF2, the polyclonal antibodies to ubiquitin showed no significant background staining in tissue sections. It is possible that DF2 reacts with both free and conjugated forms of ubiquitin (*14*), whereas the affinity-purified antibodies preferentially recognize a conjugated form. Although the target or targets of ubiquitin in PHF are unknown, it may be that phosphorylated forms of tau that are undetectable in control brains (*5*) are linked to ubiquitin in PHF. Smearing on immunoblots could be attributed to ubiquitination (*15*) of altered forms of phosphorylated tau in PHF.

Our data suggest that PHF are not inert elements within degenerating neurons; tangle-bearing neurons are actively responding by ubiquitinating PHF proteins. The failure of degradation of PHF in spite of ubiquitination could be due to a defective ATP-dependent protease or to an unusual resistance of PHF to the protease (*7*).

Recently, the ubiquitin and ATP-dependent proteolysis has been highlighted in connection with the heat-shock response. The overloading of the proteolysis system by abnormal proteins seems to activate heat-shock genes (*16*). Thus, one may speculate that accumulated PHF would trigger the expression of heat-shock genes in tangle-bearing neurons. Recently, constitutive expression of heat-shock proteins was observed in indirect flight muscles of certain *Drosophila* mutants that produce abnormal forms of actin III (*17*). In view of these data, it is tempting to speculate that PHF-bearing neurons could express heat-shock proteins constitutively at least at certain stages of neuronal degeneration. If so, AD-specific neuronal proteins that are currently being intensively searched for in numerous laboratories might be found among heat-shock proteins.

REFERENCES AND NOTES

1. M. Kidd, *Nature (London)* **197**, 192 (1963); H. Wisniewski, H. K. Narang, R. D. Terry, *J. Neurol. Sci.* **27**, 173 (1976).
2. B. E. Tomlinson, G. Blessed, M. Roth, *J. Neurol. Sci.* **11**, 205 (1970); G. K. Wilcock and M. M. Esiri, *ibid.* **56**, 343 (1982).
3. D. J. Selkoe, Y. Ihara, F. J. Salazar, *Science* **215**, 1243 (1982).
4. Y. Ihara, C. Abraham, D. J. Selkoe, *Nature (London)* **304**, 727 (1983).
5. J. P. Brion, Ph. van den Bosch de Aguilar, J. Flament-Durand, paper presented at the International Tropon-Bayer-Symposium, "Aging of the brain," Cologne, F.R.G., 13 to 16 November 1984; I. Grundke-Iqbal *et al.*, *J. Biol. Chem.* **261**, 6084 (1986); N. Nukina and Y. Ihara, *J. Biochem.* **99**, 1541 (1986); Y. Ihara, N. Nukina, R. Miura, M. Ogawara, *ibid.*, p. 1807; J. G. Wood, S. S. Mirra, N. J. Pollock, L. I. Binder, *Proc. Natl. Acad. Sci. U.S.A.* **83**, 4040 (1986); K. S. Kosik, C. L. Joachim, D. J. Selkoe, *ibid.*, p. 4044; I. Grundke-Iqbal *et al.*, *ibid.*, p. 4913.
6. G. Goldstein *et al.*, *Proc. Natl. Acad. Sci. U.S.A.* **72**, 11 (1975). The molecular weight of DF2 antigen was estimated as approximately 5000 on a 15% polyacrylamide gel (Laemmli). The discrepancy between this estimated and the calculated molecular weight of ubiquitin (8565) is presumably due to its anomalous mobility in this gel system. Similarly, A. L. Haas and K. D. Wilkinson [*Prep. Biochem.* **15**, 49 (1985)] also estimated the molecular weight of ubiquitin as 5.5 kD.
7. D. J. Selkoe, Y. Ihara, C. Abraham, C. G. Rasool, A. H. McCluskey, *Banbury Rep.* **15**, 125 (1983).
8. T. Masaki, M. Tanabe, K. Nakamura, M. Soejima, *Biochim. Biophys. Acta* **660**, 44 (1981); *ibid.*, p. 51; T. Masaki, T. Fujihashi, M. Soejima, *Nogeikagaku* **58**, 865 (1984). One of the features of lysylendopeptidase is its remarkable resistance to detergents and denaturants. The protease is active even in the presence of 5*M* urea.
9. Electron microscopy of the PHF fraction showed that PHF were by far the major constituent, which were absent in the final fraction from control brain. The main contaminants were large and small particles of various densities. Occasionally intact amyloid cores and their fragments were also observed.
10. H. Mori and Y. Ihara, unpublished data.
11. D. H. Schlesinger, G. Goldstein, H. D. Niall, *Biochemistry* **14**, 2214 (1975).
12. A. Hershko, A. Ciechanover, H. Heller, A. L. Haas, I. A. Rose, *Proc. Natl. Acad. Sci. U.S.A.* **77**, 1783 (1980); A. L. Haas and I. A. Rose, *ibid.* **78**, 6845 (1981); A. Hershko, H. Heller, S. Elias, A. Ciechanover, *J. Biol. Chem.* **258**, 8206 (1983).
13. A. L. Haas and P. M. Bright, *J. Biol. Chem.* **260**, 12464 (1985).
14. The epitope of DF2 was shown by means of the dot immunobinding method and ubiquitin fragments to reside in U-6. The two synthetic peptides:

$$\overset{32}{\text{Asp-Lys-Glu-Gly-Ile-Pro-Pro-}}\overset{39}{\text{Asp}}$$

and

$$\overset{45}{\text{Phe-Ala-Gly-Lys-Gln-Leu-Glu-Asp-}}\overset{53}{\text{Gly}}$$

did not react with DF2. Hence we speculate further that the epitope of DF2 would be

$$\overset{40}{\text{Gln-Gln-Arg-Leu-}}\overset{44}{\text{Ile}}\text{ in U-6}$$

15. D. Finley, A. Ciechanover, A. Varshavsky, *Cell* **37**, 43 (1984).
16. J. Ananthan, A. L. Goldberg, R. Voellmy, *Science* **232**, 522 (1986); S. Munro and H. Pelham, *Nature (London)* **317**, 477 (1985).
17. C. C. Karlik, M. D. Coutu, E. A. Fyrberg, *Cell* **38**, 711 (1984); Y. Hiromi and Y. Hotta, *EMBO J.* **4**, 1681 (1985).

18. We thank A. L. Haas for providing affinity-purified antibodies to ubiquitin, D. J. Selkoe for helpful comments, and T. Seki for technical assistance. Supported in part by a grant-in-aid for scientific research from the Ministry of Education, Science, and Culture of Japan.

17 September 1986; accepted 16 January 1987

Regional Changes in Calcium Underlying Contraction of Single Smooth Muscle Cells

DAVID A. WILLIAMS,* PETER L. BECKER, FREDRIC S. FAY

The role of calcium in regulating the contractile state of smooth muscle has been investigated by measuring calcium and contraction in single smooth muscle cells with the calcium-sensitive dye fura-2 and the digital imaging microscope. The concentration of free calcium in the cytoplasm increased after stimulation of the cells by depolarization with high potassium or by application of carbachol. Changes in calcium always preceded contraction. The increase in calcium induced by these stimuli was limited to less than 1 μ*M*. Calcium within the nucleus was also subject to a limitation of its rise during contraction. Intranuclear calcium rose from 200 n*M* at rest to no more than 300 n*M* while cytoplasmic calcium rose to over 700 n*M*. These apparent ceilings for both cytoplasmic and intranuclear calcium may result either from negative feedback of calcium on cytoplasmic and nuclear calcium channel gating mechanisms, respectively, or from the presence of calcium pumps that are strongly activated at the calcium ceilings.

MEASUREMENTS OF INTRACELLULAR free calcium concentrations ($[Ca^{2+}]_i$) in smooth muscle have been performed in a number of ways in intact tissues (*1*) and in populations of isolated cells (*2, 3*). In general, $[Ca^{2+}]_i$ is correlated with the extent of contraction, although several exceptions have been reported (*4*). The exceptions may reflect Ca^{2+}-independent mechanisms that control contraction of smooth muscle or, alternatively, heterogeneity in the response of cells in a multicellular population that may produce an apparent dissociation of contractile state from Ca^{2+}. The development of a new class of fluorescent indicators (*5*) that produce a large Ca^{2+}-sensitive signal provides the opportunity to circumvent these uncertainties by permitting the measurement of Ca^{2+} and contraction in the same cell. Moreover, the use of the dye fura-2 in conjunction with the digital imaging microscope allows measurement of $[Ca^{2+}]_i$ with subcellular spatial resolution (*6*). Here we use this approach to assess the magnitude and kinetics of changes in Ca^{2+} that take place in different regions of single smooth muscle cells as they contract and then relax after exposure to excitatory stimuli (*7*).

The smooth muscle cells used in these studies were isolated by enzymatic disaggregation of the stomach muscularis of the toad (*Bufo marinus*) (*8*). $[Ca^{2+}]_i$ was monitored in cells loaded with fura-2 as a change in the

Department of Physiology, University of Massachusetts Medical School, Worcester, MA 01605.

*To whom correspondence should be addressed at his present address: Department of Zoology, La Trobe University, Bundoora, Victoria, Australia 3083.

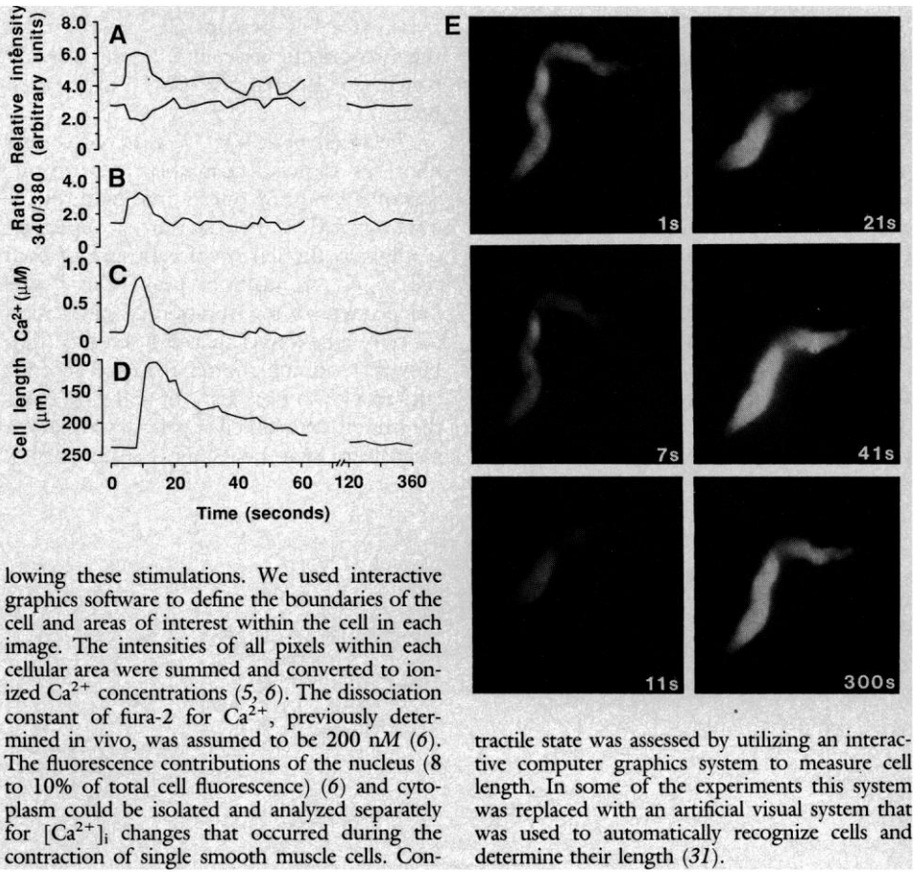

Fig. 1. Change in the cytosolic Ca^{2+} concentration during the contraction of a single smooth muscle cell in response to potassium. (**A**) 340- (upper) and 380-nm (lower) fluorescence intensities (with emission monitored at 500 nm) of the cytoplasm within a single cell that was maintained in a Hepes-based amphibian physiological solution (137 m*M* Na^+, 3 m*M* K^+, 1 m*M* Mg^{2+}, 1.8 m*M* Ca^{2+}, 112 m*M* Cl^-, 7 m*M* phosphate, 1 m*M* sulfate, and 20 m*M* Hepes. (**B**) Ratio of fluorescence intensities measured at 340- and at 380-nm excitation. (**C**) Conversion of $R_{340/380}$ values to $[Ca^{2+}]_i$. (**D**) Measurements of cell length during contraction. (**E**) Selected images, obtained during the time course with 380-nm excitation at the times indicated in seconds (s). All cell images were obtained, photographically processed, and displayed at the same gain. The time interval between dual wavelength images, as well as the number of video frames summed (*30*), was defined at the start of each experiment with an interactive digital imaging program. An electronic shutter in the illumination light path was controlled by the computer and remained open only during periods of image acquisition. In a typical experiment, two dual-wavelength image pairs of a resting cell were acquired and then, as additional image pairs continued to be collected, a micropipette (under micromanipulator control) was positioned in the cell vicinity and the cell was stimulated by (i) passing a brief electrical pulse (3*M* KCl–filled pipette) or (ii) replacing the total Na^+ concentration of the bathing medium by pressure ejection of a K^+-substituted Ringer from the pipette (iii) or by pressure ejection of concentrated acetylcholine (10^{-4}*M*). More than 80% of the elongated, relaxed cells contracted reversibly following these stimulations. We used interactive graphics software to define the boundaries of the cell and areas of interest within the cell in each image. The intensities of all pixels within each cellular area were summed and converted to ionized Ca^{2+} concentrations (*5, 6*). The dissociation constant of fura-2 for Ca^{2+}, previously determined in vivo, was assumed to be 200 n*M* (*6*). The fluorescence contributions of the nucleus (8 to 10% of total cell fluorescence) (*6*) and cytoplasm could be isolated and analyzed separately for $[Ca^{2+}]_i$ changes that occurred during the contraction of single smooth muscle cells. Contractile state was assessed by utilizing an interactive computer graphics system to measure cell length. In some of the experiments this system was replaced with an artificial visual system that was used to automatically recognize cells and determine their length (*31*).

ratio of the 510-nm fluorescence intensity at 340-nm and 380-nm excitation. The fluorescence was quantified with a silicon-intensified target (SIT) camera and a digital imaging system (*6, 9*) with the following modifications: (i) The computer-controlled filter changer was modified so that the interference filters in the excitation path could be more rapidly alternated (the switching time was less than 200 msec). (ii) The imaging software was expanded so that a number of image pairs at 340 and 380 nm, each consisting of the sum of a given number of video frames, could be automatically collected at selected intervals in time. In some experiments, we used a dual-wavelength digital microspectrofluorimeter (*10*) to provide high time resolution (~300 Hz) measurements of cellular $[Ca^{2+}]_i$ without the use of digital imaging.

Aliquots of isolated cells (300 μl) were incubated with the acetoxy methyl ester of fura-2 (fura-2/AM) (*11*) at 30°C with gentle agitation for 30 to 60 minutes in the presence of an initial concentration of 0.3 μ*M* fura-2/AM. The loading period was shorter than we have used in previous experiments and, consequently, the fluorescence contribution of the sarcoplasmic reticulum was significantly reduced; after longer loading times the sarcoplasmic reticulum is apparent as areas of high fluorescence intensity (and high $[Ca^{2+}]_i$) along the periphery of the resting cell (*6*). Loading was terminated by dilution of the cell suspension (10- to 100-fold) with a Hepes-based amphibian saline solution (Fig. 1), and the cells were then incubated for 20 minutes to facilitate complete de-esterification of internalized fura-2/AM. With loading times shorter than 30 minutes, de-esterification was incomplete: the 340/380 fluorescence ratio of cells lysed in the presence of Ca^{2+} was significantly depressed relative to that of the fully de-esterified fura-2, and spectral decomposition of the fura-2 fluorescence revealed the presence of a Ca^{2+}-insensitive component (*12*). At the end of the loading and incubation period virtually all cellular fura-2 was fully Ca^{2+}-sensitive at an intracellular concentration of between 110 and 140 μ*M* (measured in populations of cells). The levels of intracellular fura-2 indicate that the loading process was efficient; 70 to 90% of the added fura-2 was trapped and fully cleaved by these cells (*13*). At these intracellular levels, fura-2 does not appear to significantly affect intracellular Ca^{2+} buffering, in contrast to results obtained with quin2 (*14*). A further advantage of fura-2 over quin2 was that it was far more resistant to photobleaching in the digital imaging microscope (*15*). In the experiments reported here, the amount of photobleaching was negligible due to use of short light exposures and appropriate attenuation of the light source.

When a single smooth muscle cell was stimulated by potassium application (ejection duration, 2 seconds), there was a decrease in the fluorescence resulting from 380-nm excitation and a concomitant increase in the fluorescence monitored at 340-nm excitation (Fig. 1A). Changes in the 340/380 nm ratio ($R_{340/380}$) (Fig. 1B) were converted into Ca^{2+} concentrations (Fig. 1C) (*6*). Cytosolic $[Ca^{2+}]_i$ increased from 140 n*M*, before stimulation, to a peak level of 820 n*M* within 6 seconds and returned to resting level 14 seconds after the initial rise.

The time course of $[Ca^{2+}]_i$ change principally reflects the kinetics for the processes responsible for Ca^{2+} entering the cytoplasm and for restoring Ca^{2+} to its resting level rather than the kinetics of delivery and removal of excitatory stimuli. This follows from the observation that the rise in $[Ca^{2+}]_i$ after K^+ stimulation is considerably slower than the rate of K^+ delivery from the micropipette (*16*), and that similar rates of fall in $[Ca^{2+}]_i$ are seen after K^+ and electrical stimulation ($t_{1/2}$ for decay, 4.5 and 6 seconds, respectively). The Ca^{2+} and contractile response to K^+ stimulation both require extracellular Ca^{2+}; they are both rapidly ($t_{1/2} < 30$ seconds) and almost totally suppressed when the extracellular Ca^{2+} is below 100 n*M* (*2, 17*). The isosmotic replacement of extracellular Na^+ by K^+ results in a sustained depolarization of the cell mem-

brane from its normal resting potential of −55 mV (*18*), leading to activation of voltage-sensitive Ca^{2+} channels and an increase in cytosolic $[Ca^{2+}]_i$ (*19*). The amount of Ca^{2+} expected to enter from sustained depolarization to 0 mV ranges from 19 to 53 μmol per liter of cell H_2O in toad stomach muscle cells (*20*). In order for $[Ca^{2+}]_i$ to change from 140 to 820 n*M* in a cell containing 125 μ*M* fura-2, an additional 49 μmol of Ca^{2+} per liter of cell H_2O must bind to the fura-2. Bond *et al.* (*21*) suggest that smooth muscle has an endogenous Ca^{2+} buffering capacity of at least 100 μ*M*. Thus, additional sources of Ca^{2+} are probably necessary to account for the observed rise in $[Ca^{2+}]_i$—perhaps Ca^{2+} release from the sarcoplasmic reticulum, an inwardly directed sarcolemmal Na^+-Ca^{2+} exchange, or both.

The mean peak $[Ca^{2+}]_i$ achieved during high K^+ stimulation in these experiments was 690 ± 42 n*M* (mean ± SEM throughout; $n = 13$). If the data are grouped according to the length of exposure of each cell to K^+ stimulation, peak $[Ca^{2+}]_i$ was independent of the duration of stimulation for transients longer than 5.0 seconds (*22*). However, stimuli shorter than 5.0 seconds elicited a lower peak Ca^{2+} of 450 n*M*. Thus, the smooth muscle cell apparently contains a mechanism that limits the rise in $[Ca^{2+}]_i$ after stimulation by K^+. A limit to steady-state $[Ca^{2+}]_i$ during long exposure (1 to 5 minutes) to step increases in K^+ has also been seen in this cell type with Ca^{2+}-sensitive microelectrodes (*18*). The rise in $[Ca^{2+}]_i$ in response to other stimuli such as a maximum carbachol concentration (10^{-4}*M*) may be similarly limited, as the average level achieved (800 n*M*) is similar to that seen in response to K^+. Electrical stimulation induces an increase in $[Ca^{2+}]_i$ that exceeds this Ca^{2+} limiting mechanism (Fig. 2). However, high time-resolution analysis reveals that the rate of rise in $[Ca^{2+}]_i$ after electrical stimulation is often reduced when the $[Ca^{2+}]_i$ is higher than the ceiling that exists during K^+ stimulation (Fig. 2). The continued rise in $[Ca^{2+}]_i$ after electrical stimulation may reflect the induction of additional pathways for Ca^{2+} entry into the cell—perhaps the nonspecific increase in cell permeability that occurs after application of strong electric fields (*23*). The ability to record a $[Ca^{2+}]_i$ in excess of the K^+-induced Ca^{2+} ceiling indicates that the ceiling is not a trivial reflection of dye saturation by Ca^{2+}.

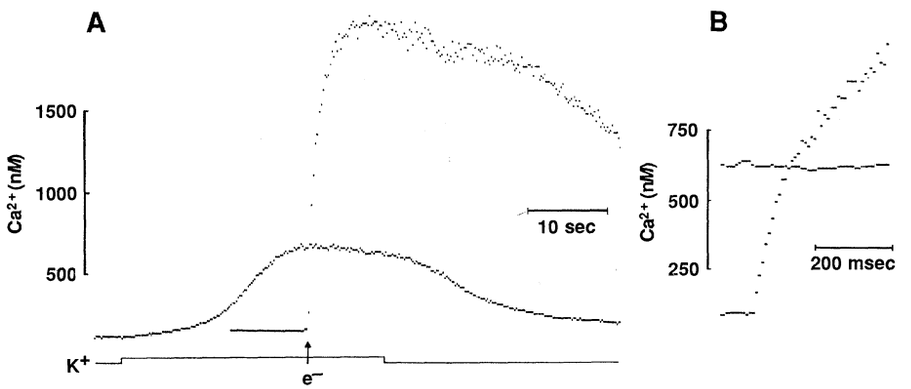

Fig. 2. High time-resolution microspectrofluorimeter measurement of $[Ca^{2+}]_i$ in single smooth muscle cells after either K^+ application or brief electrical stimulation. K^+ was administered as in Fig. 1. Electrical stimulation was via small platinum wires positioned 100 μm on either side of the cell. Single 100-V, 100-μsec pulses were applied by a Grass model SD9 stimulator. The cell was alternately illuminated by 340- and 380-nm light at a frequency of 125 Hz. The microscope image was masked at an intermediate image plane to block all but the cell image and a small surrounding area. The image was then diverted through a 500-nm interference filter (30-nm band pass) to the photo cathode of a photomultiplier tube operating in photon counting mode. A ratio signal ($R_{340/380}$) was obtained by division of successive 340- and 380-nm excitation photon counts (each corrected for background counts obtained in the same manner with no cell in view). The resulting ratio was converted to $[Ca^{2+}]_i$ with maximum $R_{340/380}$, minimum $R_{340/380}$, and β values obtained when viewing fura-2–free acid in the standard calibration solutions (*6*). (**A**) The response of $[Ca^{2+}]_i$ to a prolonged K^+ application. Peak $[Ca^{2+}]_i$ (625 n*M*) is maintained for the duration of the stimulus and returns to prestimulus levels (100 n*M*) after the cessation of stimulation. In contrast, Ca^{2+} increased to a much higher level (~2 μ*M*) in the same cell following a single brief electrical stimulus (e^-) (also shown in A). (**B**) An expanded view of the cross-over of the Ca^{2+} responses seen in (A). The rise in $[Ca^{2+}]_i$ after electrical stimulation has two distinct phases—an initial rapid phase (average rate, 8 n*M*/msec) followed by a much slower phase (1.6 n*M*/msec). The inflection seems to occur as Ca^{2+} passes through the concentration range that represents the ceiling to $[Ca^{2+}]_i$ apparent after K^+ application in the same cell (625 n*M*).

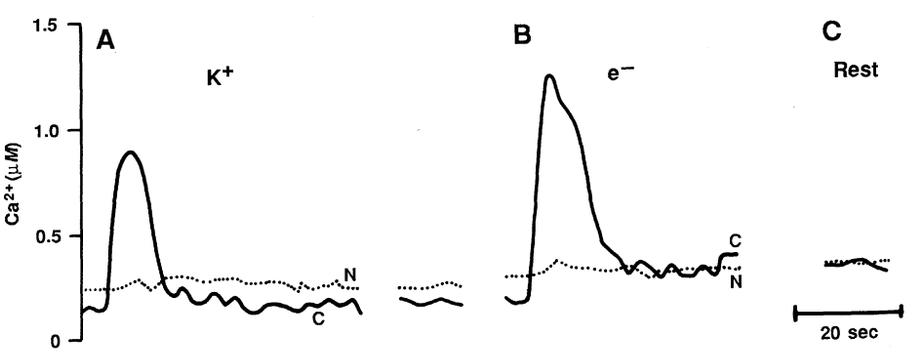

Fig. 3. Measurements of nuclear (N) and cytosolic (C) $[Ca^{2+}]_i$ after depolarizing stimuli. (**A**) K^+ stimulation. (**B**) Electrical pulse (100 V, 0.1 msec) stimulation (e^-). The cell was allowed to rest several minutes between stimuli and after electrical stimulation. (**C**) Representative Ca^{2+} shown for rest periods.

Changes in cytoplasmic $[Ca^{2+}]_i$ in response to stimulation by K^+ depolarization or carbachol are well below the 2 to 3 μ*M* level found to be necessary to fully activate contraction in saponin-skinned smooth muscle cells (*26*). This suggests that the $[Ca^{2+}]$ ceiling may prevent full activation of the contractile machinery. Alternatively, this may indicate differences between the Ca^{2+} sensitivity of the contractile apparatus of skinned cells and that of intact cells, due to the loss of an unknown Ca^{2+}-sensitizing inotropic agent during skinning.

The transition from resting to elevated

$[Ca^{2+}]_i$ in response to K^+ or carbachol is followed by active shortening of the smooth muscle cell (Fig. 1D). The onset of cell shortening after stimulation with high K^+ occurred 3 seconds after the first detectable rise in $[Ca^{2+}]_i$. A reduction in the intensity of the 380-nm cell image, consonant with a $[Ca^{2+}]_i$ increase, occurred before the first perceptible change in cell length (Fig. 1E). The mean delay (1.6 ± 0.4 seconds, n = 11) between the onset of K^+ stimulation (as marked by the initiation of the rise in Ca^{2+}) and beginning of cell shortening is considerably longer than that previously reported between the onset of force development and supramaximal electrical stimulation (0.214 ± .013 second) (*27*). To some extent this difference may be due to the method of stimulation because the mean delay between electrical stimulation and the onset of shortening in this study was 0.7 ± 0.4 second (n = 6). Cell shortening was maximal 3 seconds after peak $[Ca^{2+}]_i$ was recorded and was greater than 80% of the maximal length change (135 μm) at the time Ca^{2+} had returned to prestimulus levels. Cells were able to relax close to their initial length and configuration in the absence of any external restoring force (Fig. 1E). The half time for re-extension of cells stimulated with high K^+ averaged 20 ± 4 seconds (n = 11).

Thus, these results indicate that Ca^{2+} changes are centrally involved in excitation-contraction coupling in smooth muscle. The changes in $[Ca^{2+}]_i$ that follow K^+, carbachol, or electrical stimulation are uniform throughout the cytoplasm within the 0.5-second temporal resolution of the imaging system. However, Ca^{2+} gradients are observed between the nucleus and cytoplasm in resting and contracting cells (Fig. 3) (*6*). As cytoplasmic Ca^{2+} is elevated by large, sustained changes in the concentration of Ca^{2+} in the extracellular medium, nuclear Ca^{2+} rises less from its normal level (220 n*M*) to approximately 350 n*M* (*6*). Therefore, a mechanism in the nuclear membranes regulating $[Ca^{2+}]$ might function during contraction to screen the nucleus from fluctuations in cytoplasmic Ca^{2+}. The analysis reported here provided an opportunity for directly testing this suggestion by measuring the changes in $[Ca^{2+}]_i$ in both cytoplasm and nucleus after K^+ and electrical stimulation (Fig. 3). These results are typical of five cells in which the nucleus could be clearly distinguished throughout a contraction-relaxation cycle. Whereas cytoplasmic $[Ca^{2+}]_i$ rose above 800 n*M* during stimulation, intranuclear Ca^{2+} was unchanged until well into the cytosolic Ca^{2+} transient and achieved a peak level of approximately 300 to 350 n*M*. The different peak Ca^{2+} concentrations and the different time courses indicate that the nuclear Ca^{2+} concentrations do not passively follow changes in cytosolic Ca^{2+} and that the nuclear envelope may protect the nucleus from the fluctuations in cytoplasmic Ca^{2+} that initiate and maintain contraction. If, as has been suggested, some intranuclear processes are regulated by Ca^{2+} (*28*), then screening the nuclear environment from cytoplasmic Ca^{2+} changes would prevent the inappropriate triggering of these intranuclear processes during contraction. The mechanism of this effect is unknown. Cytoplasmic Ca^{2+} may act through negative feedback on nuclear membrane Ca^{2+} permeability, as it does on the plasma membrane of these cells (*2*) and for membranes of other excitable cells (*24, 29*). Alternatively, activation of a Ca^{2+} transport system in the nuclear envelope that is strongly activated beyond 300 n*M* $[Ca^{2+}]_i$ may be responsible for the observed limit on intranuclear Ca^{2+} changes.

REFERENCES AND NOTES

1. C. M. Rembold and R. A. Murphy, *Circ. Res.* **58**, 803 (1986); I. R. Neering and K. G. Morgan, *Nature (London)* **288**, 585 (1980); J. P. Morgan and K. G. Morgan, *Pfluegers Arch.* **395**, 75 (1982).
2. D. A. Williams and F. S. Fay, *Am. J. Physiol.* **250**, C799 (1986).
3. S. Kobayashi, M. Kanaide, M. Nakamura, *Science* **229**, 553 (1985); K. N. Bitar, P. G. Bradford, J. W. Putney, G. M. Makhlouf, *ibid.* **232**, 1143 (1986); F. S. Fay, H. H. Schlevin, W. C. Granger, S. R. Taylor, *Nature (London)* **280**, 506 (1979).
4. J. P. Morgan and K. G. Morgan, *J. Physiol. (London)* **351**, 155 (1984); T. DeFeo and K. G. Morgan, *ibid.* **369**, 269 (1985).
5. G. Grynkiewicz, M. Poenie, R. Y. Tsien, *J. Biol. Chem.* **260**, 3440 (1985).
6. D. A. Williams, K. E. Fogarty, R. Y. Tsien, F. S. Fay, *Nature (London)* **318**, 558 (1985).
7. Sections of this work have previously been communicated. D. A. Williams, K. E. Fogarty, R. Y. Tsien, F. S. Fay, *J. Gen. Physiol.* **86**, 37a (1985); D. A. Williams, K. E. Fogarty, F. S. Fay, *Biophys. J.* **49**, 464a (1986); *J. Gen. Physiol.* **88**, 61a (1986).
8. F. S. Fay, R. Hoffman, S. LeClair, P. Merriam, *Methods Enzymol.* **85**, 284 (1982).
9. F. S. Fay, K. E. Fogarty, J. M. Coggins, in *Optical Methods in Cell Physiology*, P. DeWeer and B. Salzburg, Eds. (Wiley, New York, 1986), p. 51.
10. J. F. Hatch, D. A. Williams, K. E. Fogarty, F. S. Fay, *Biophys. J.* **49**, 464a (1986); P. L. Becker, J. F. Hatch, K. E. Fogarty, F. S. Fay, *J. Gen. Physiol.* **88**, 11a (1986).
11. Stock solutions of fura-2/AM were generally 1.0 m*M* in dimethylsulfoxide and were stored at −40°C. Integrity of the stock solution was periodically checked on a Spex CM-1 spectrofluorimeter for time-dependent hydrolysis of esterified fura-2/AM.
12. M. Scanlon, D. A. Williams, F. S. Fay, *J. Gen. Physiol.* **88**, 52a (1986). In vitro cleavage of fura-2/AM by commercially available esterase (Sigma) has revealed the existence of an intermediate that is also transiently observed during the early stages of loading of cell suspensions. This species is virtually insensitive to Ca^{2+}, and displays the spectral characteristics necessary to explain the difference between total and Ca^{2+}-sensitive fura-2 measurements. This component does not represent fura-2/AM or similar species that are trapped in internal compartments as selective lysis of the plasma membrane with digitonin is able to liberate all of the dye in the cells.
13. For estimates of loading efficiency: average cell volume, 7.85×10^{-12} liters; loading concentration, $3 \times 10^{-7}M$; cell density, 2.5×10^8 cells per liter; loading volume, 1×10^{-3} liters. The expected maximum cellular fura-2 concentration, assuming that cells trap all added dye molecules, should therefore be: maximum intracellular fura-2 concentration = loading concentration × [total volume/(number of cells × average cell volume)] = $3 \times 10^{-7}M \times 1 \times 10^{-3}/(2.5 \times 10^5 \times 7.85 \times 10^2) = 153$ μ*M*. Loading efficiency would then be the calculated intracellular fura-2 concentration divided by the maximum possible fura-2 concentration.
14. The time course and magnitude of contraction after K^+, carbachol, or electrical stimulation was not altered in fura-2–loaded versus nonloaded cells. This is in contrast to the results of a previous study with quin2-loaded smooth muscle cells (*2*), where higher dye concentrations were necessary to obtain a measurable fluorescent signal.
15. The fluorescent intensity of single smooth muscle cells loaded with quin2 declines by over 50% with 90 seconds of continuous 340-nm illumination (unattenuated) on our digital imaging microscope, whereas fura-2 fluorescence declines less than 10% under the same conditions.
16. To simulate the kinetics of increasing the K^+ concentration surrounding the cell after pressure application from a micropipette, we ejected fura-2 (pentapotassium salt) from a typical micropipette into a Ca^{2+}-containing medium placed over the objective of a microscope-based high time-resolution microspectrofluorimeter (*10*). The rise time ($t_{1/2}$ = 1 second) for fluorescence intensity, recorded with a photomultiplier tube at 340 nm, gave an approximate measure of the time to increase K^+ in the cell vicinity (P. L. Becker, D. A. Williams, F. S. Fay, unpublished observations).
17. Fura-2; D. A. Williams and F. S. Fay, unpublished observations.
18. H. Yamaguchi, *Cell Calcium* **7**, 203 (1986).
19. J. V. Walsh and J. Singer, *Am. J. Physiol.* **239**, C162 (1980).
20. Our manual integration of the Ca^{2+} current trace (Fig. 3 from L. H. Clapp, M. B. Vivaudou, J. J. Singer, J. V. Walsh, *Proc. Natl. Acad. Sci. U.S.A.*, in press) indicates that about 36 picocoulombs of charge can enter a single toad stomach muscle cell within 3 seconds after the membrane potential is stepped from −89 mV to +9 mV. Figure 2 of that paper suggests that the total charge could be as high as 102 picocoulombs. This represents a Ca^{2+} influx of $(36 \text{ to } 102) \times 10^{-12}/(2 \times 96{,}487 \times 10^{-11}) =$ 19 to 53 μmol of Ca^{2+} per liter of cell H_2O; where 96,487 = Faraday's constant; 2 = valence of Ca^{2+}; and 10^{-11} = average cell volume in liters.
21. M. Bond, H. Shuman, A. P. Somlyo, A. V. Somlyo, *J. Physiol. (London)* **357**, 185 (1984).
22. The width at half maximum of the peak $[Ca^{2+}]_i$ was used as an indicator of the relative duration of stimulation for different cells. The mean peak Ca^{2+} was 730 n*M* (n = 2) for transients 5.0 seconds at half amplitude and 740 ± 50 n*M* (n = 6) for transients 6.9 seconds at half amplitude and 680 n*M* (n = 2) for transients 8.5 seconds at half amplitude.
23. U. Zimmermann and J. Greyson, *Biotechniques*, **1** (3), 118 (1983).
24. A. Fabiato, *Am. J. Physiol.* **245**, C1 (1983); D. Tillotson, *Proc. Natl. Acad. Sci. U.S.A.* **76**, 1497 (1979); R. Eckert and J. Chad, *Prog. Biophys. Mol. Biol.* **44**, 215 (1984).
25. K. Kamm and J. T. Stull, *Annu. Rev. Pharmacol. Toxicol.* **25**, 593 (1985); C. R. Scheid and F. S. Fay, *Am. J. Physiol.* **246**, C422 (1984); A. K. Grover, *Cell Calcium* **6**, 227 (1985).
26. G. J. Kargacin and F. S. Fay, *J. Gen. Physiol.*, in press.
27. F. S. Fay, *Nature (London)* **265**, 553 (1977).
28. B. A. White, *J. Biol. Chem.* **260**, 1213 (1985); E. T. Maizels and R. A. Jungmann, *Endocrinology* **112**, 1895 (1983); N. Sahyoun, H. Levine, P. Cuatrecasas, *Proc. Natl. Acad. Sci. U.S.A.* **81**, 4311 (1984); N. Sahyoun, H. Levine, D. Bronson, P. Cuatrecasas, *J. Biol. Chem.* **259**, 9341 (1984).
29. A. Fabiato, *Acta Physiol. Scand. Suppl.* **508**, 16 (1982).
30. Typically 16 frames per image were summed at each wavelength to achieve a sufficient degree of certainty in our $[Ca^{2+}]_i$ measurements. Average standard deviation for $[Ca^{2+}]_i$ in an image of a resting smooth muscle cell was ±12 n*M*. This estimate of uncertainty in the Ca^{2+} concentration is based upon analysis of the noise associated with the imaging process for a single pixel in a resting smooth muscle cell in which 128 video frames are summed and averaged. The expected uncertainty in Ca^{2+} concentration for each pixel would increase by a factor of 2.2 for an image comprised of the sum of 16 video

frames, as used for these dynamic studies. $[Ca^{2+}]_i$ was calculated for these studies by summing all pixels in the cytoplasm in the 340- and 380-nm images. This process would be expected to decrease the uncertainty by 67 times for a typical cell.

31. S. B. Abramson, K. E. Fogarty, F. S. Fay, in preparation. Cell lengths were determined by defining the central axis of the cell in each image of a series with interactive computer graphics software. The number of pixels that constituted this axis was then converted to an actual measurement of cell length by reference to a conversion scale (pixels per micrometer) with correction for the aspect ratio of each pixel within the axis. Fluorescence intensities (at each excitation wavelength) were calculated with a joystick-driven, interactive graphics software routine to define areas of interest within each image (for example, cell boundaries and the nuclear-cytosol interface). All pixel intensities within the cytosol and nucleus were summed. The fluorescence ratios were then calculated for the nucleus or cytoplasm as a whole by dividing the total fluorescence (measured in a particular area at 340 nm) by the same measure made at 380 nm. Ratios based on division on a pixel-by-pixel basis were not calculated during contraction as such images are subject to severe distortion due to the motion of the cell between consecutive 340- and 380-nm images. As fluorescence could not be measured simultaneously at each wavelength, a ratio was determined by the division of the intensities within a given 340-nm image by those resulting from an interpolation between the 380-nm images that preceded and followed this image.

32. We thank K. E. Fogarty and S. B. Abramson for development of software essential to the performance of this work; L. J. Harris for technical expertise; R. Hutchinson for clerical assistance; and G. J. Kargacin, S. M. Sims, and J. J. Singer for critical reading and discussions. D.A.W. was supported by fellowships from the National Heart Foundation of Australia and the American Heart Association (Massachusetts affiliate); P.L.B. was supported by NIH fellowship AM07807. Supported by NIH grant HL-14523 and by a grant from the Muscular Dystrophy Association.

23 October 1986; accepted 23 January 1987

A New Probe for the Diagnosis of Myotonic Muscular Dystrophy

R. J. BARTLETT,* M. A. PERICAK-VANCE, L. YAMAOKA, J. GILBERT, M. HERBSTREITH, W.-Y. HUNG, J. E. LEE, T. MOHANDAS, G. BRUNS, C. LABERGE, M.-C. THIBAULT, D. ROSS, A. D. ROSES

Myotonic muscular dystrophy (DM) is the most common muscular dystrophy, affecting adults as well as children. It is inherited as an autosomal dominant trait and is characterized by variable expressivity and late age-of-onset. Linkage studies have established the locus on chromosome 19. In order to identify tightly linked probes for diagnosis as well as to define in detail the DM gene region, chromosome 19 libraries were constructed and screened for restriction fragment length polymorphisms tightly linked to DM. A genomic clone, LDR152 (D19S19), was isolated that is tightly linked to DM; recombination fraction = 0.0 (95% confidence limits 0.0–0.03); lod score, 15.4.

MYOTONIC DYSTROPHY (DM) IS the most common form of adult and childhood muscular dystrophy. It is inherited as an autosomal dominant trait located on chromosome 19. There have been no documented cases of new mutation (*1*). Multiple very large families have been evaluated clinically and genotyped by means of both serum and DNA polymorphisms in a linkage strategy designed to identify loci tightly linked to the disease. Six large clinically studied DM families were used in the linkage analysis. Thus far over 400 individuals have been genotyped. The apolipoprotein C2 (ApoC2) locus has been closely linked to DM (*2, 3*). Although approximately 96 to 98% accurate for diagnosis, it is too far from the DM locus to be a starting point for the physical techniques of chromosome walking and/or hopping to isolate the gene. We therefore screened restriction fragment length polymorphisms (RFLPs) on chromosome 19 (CH19) in these families in order to identify a more tightly linked marker. New probe testing was dependent upon the absence of detectable crossover events and was focused toward defining the DM gene region rather than mapping CH19.

A flow-sorted, genomic DNA library enriched for CH19, was prepared from a human lymphoblast cell line established by Epstein-Barr virus transformation of white blood cells from a normal female. A bivariate flow karyogram of a typical preparation is shown in Fig. 1A. Since CH19 represents only 2.2% of the human genome and only 1.1% of the preparation in Fig. 1A, chromosome preparations were enriched by fractionation on linear rate zonal sucrose gradients. For comparison, analyses of fractions obtained from both the dense and less dense regions of a typical gradient demonstrate enrichment of chromosomes of groups B and C in one and enrichment of chromosomes in groups E, F, and G in the other (Fig. 1, B and C, respectively). The inherent sorting efficiency of the fractions from Fig. 1C would therefore be much greater for CH19 than the total complement (Fig. 1A). In addition to the size enrichment, the sucrose gradients removed the interphase nuclei from the chromosome fractions since nuclei pellet through the gradient during the first few minutes of centrifugation.

Fractions enriched in group F were pooled from six gradients and submitted to preparative bivariate flow sorting. Fluorescence analysis (630× power) of a sample of sorted chromosomes indicated that 53/57 (93%) were CH19, 3/57 were CH21, and 1/57 was an unidentifiable fragment. Therefore, cloning the DNA derived from sorting CH19 under these same configurations should significantly enrich for clones localized to CH19.

Genomic DNA was prepared from 1.3×10^6 flow-sorted CH19 and digested completely with Hind III. This DNA was cloned into the Hind III insertion site in Charon 21A. A total of 5.0×10^6 plaque-forming units were obtained from the packaging reaction. After screening phage plaques that had been transferred to filters (*4*) with total human DNA, small preparations (mini-lysates) from each of 403 nonhybridizing clones were digested with Hind III (Fig. 2A). Of 69 inserts determined to be free of human repeat DNA and ranging in size from 930 to 7800 bp, 30 were screened against hybrid cell panels (Fig. 3). Four regions of CH19 were distinguished and these represented approximately four equal increments of the chromosome.

Clone LDR152 (Fig. 2A, lane 5) is a 1.60-kbp Hind III fragment that maps to the proximal long-arm of CH19 (Figs. 2B and 3). The insert was not digested by Bam HI, Bst NI, Bst XI, Eag I, Eco RI, Eco RV, Hind III, Not I, Pst I, Sac I, Sac II, Sal I, Sfi I, Spe I, Taq I, Xba I, Xho I, or Xmn I. Screening of LDR152 for DNA polymorphisms was successful for Msp I and Pst I (Fig. 4A). In the case of the Msp I polymorphism, the alleles were 2.3 and 1.3 kb in size (gene frequencies were 0.15 and 0.85, respectively). The alleles for the Pst I polymorphism were 19 and 11 kb in size (gene frequencies were 0.14 and 0.86, respectively). Gene frequencies were calculated on the

R. J. Bartlett, M. A. Pericak-Vance, L. Yamaoka, J. Gilbert, M. Herbstreith, W.-Y. Hung, A. D. Roses, Department of Medicine, Neurology Division, Duke University Medical Center, Durham, NC 27710.
J. E. Lee, Department of Psychiatry, Duke University Medical Center, Durham, NC 27710.
T. Mohandas, Harbor UCLA Medical Center, Los Angeles, CA 90509.
G. Bruns, Childrens Hospital, Boston, MA 02115.
C. Laberge and M.-C. Thibault, Laval University, Quebec, Canada, G1V 462.
D. Ross, Concord Hospital, Concord 2139, New South Wales, Australia.

*To whom correspondence should be sent.